NASA/TM-20230014072



Lunar LTE Studies DRATS 2022 Report

Aaron J. Swank, Michael J. Zemba, Taylor C. Pember, Cameron M. Seidl,
Kerry J. Johnson, Nicholas C. Varaljay, and Aaron J. Yingling
Glenn Research Center, Cleveland, Ohio

Sean W. Caldwell
HX5, LLC, Cleveland, Ohio

October 2023

NASA STI Program . . . in Profile

Since its founding, NASA has been dedicated to the advancement of aeronautics and space science. The NASA Scientific and Technical Information (STI) Program plays a key part in helping NASA maintain this important role.

The NASA STI Program operates under the auspices of the Agency Chief Information Officer. It collects, organizes, provides for archiving, and disseminates NASA's STI. The NASA STI Program provides access to the NASA Technical Report Server—Registered (NTRS Reg) and NASA Technical Report Server—Public (NTRS) thus providing one of the largest collections of aeronautical and space science STI in the world. Results are published in both non-NASA channels and by NASA in the NASA STI Report Series, which includes the following report types:

- TECHNICAL PUBLICATION. Reports of completed research or a major significant phase of research that present the results of NASA programs and include extensive data or theoretical analysis. Includes compilations of significant scientific and technical data and information deemed to be of continuing reference value. NASA counter-part of peer-reviewed formal professional papers, but has less stringent limitations on manuscript length and extent of graphic presentations.

- TECHNICAL MEMORANDUM. Scientific and technical findings that are preliminary or of specialized interest, e.g., "quick-release" reports, working papers, and bibliographies that contain minimal annotation. Does not contain extensive analysis.

- CONTRACTOR REPORT. Scientific and technical findings by NASA-sponsored contractors and grantees.

- CONFERENCE PUBLICATION. Collected papers from scientific and technical conferences, symposia, seminars, or other meetings sponsored or co-sponsored by NASA.

- SPECIAL PUBLICATION. Scientific, technical, or historical information from NASA programs, projects, and missions, often concerned with subjects having substantial public interest.

- TECHNICAL TRANSLATION. English-language translations of foreign scientific and technical material pertinent to NASA's mission.

For more information about the NASA STI program, see the following:

- Access the NASA STI program home page at http://www.sti.nasa.gov

- E-mail your question to help@sti.nasa.gov

- Fax your question to the NASA STI Information Desk at 757-864-6500

- Telephone the NASA STI Information Desk at 757-864-9658

- Write to:
  NASA STI Program
  Mail Stop 148
  NASA Langley Research Center
  Hampton, VA 23681-2199

NASA/TM-20230014072



Lunar LTE Studies DRATS 2022 Report

Aaron J. Swank, Michael J. Zemba, Taylor C. Pember, Cameron M. Seidl,
Kerry J. Johnson, Nicholas C. Varaljay, and Aaron J. Yingling
Glenn Research Center, Cleveland, Ohio

Sean W. Caldwell
HX5, LLC, Cleveland, Ohio

National Aeronautics and
Space Administration

Glenn Research Center
Cleveland, Ohio 44135

October 2023

Acknowledgments

This work was supported by the National Aeronautics and Space Administration (NASA) Space Communications and Navigation program in the Space Operations Mission Directorate. The work was performed as part of the Lunar LTE Studies (LunarLiTES) project at the NASA Glenn Research Center. The authors are grateful to the Babbitt Ranches for granting use of the land as well as for supporting land-use ethics and long-term land stewardship and conservation. The authors would also like to acknowledge the support received from the United States Geological Survey (USGS) in Flagstaff and the individuals at the USGS Astrogeology Science Center, who provided logistical support and digital elevation maps of the test region. The authors thank the NASA Johnson Space Center (JSC) Desert Research and Technology Studies (DRATS) team for the over-all event organization, including team coordination, safety and logistical support. In addition, the authors would like to thank the teams from Nokia Corporation, Vinco Inc. and the JSC Avionic Systems Division who coordinated side-by-side field testing of WiFi and 4G LTE.

This report contains preliminary findings, subject to revision as analysis proceeds.

Trade names and trademarks are used in this report for identification only. Their usage does not constitute an official endorsement, either expressed or implied, by the National Aeronautics and Space Administration.

Level of Review: This material has been technically reviewed by technical management.

This report is available in electronic form at https://www.sti.nasa.gov/ and https://ntrs.nasa.gov/

Lunar LTE Studies DRATS 2022 Report

Aaron J. Swank, Michael J. Zemba, Taylor C. Pember, Cameron M. Seidl,
Kerry J. Johnson, Nicholas C. Varaljay, and Aaron J. Yingling
National Aeronautics and Space Administration
Glenn Research Center
Cleveland, Ohio 44135

Sean W. Caldwell
HX5, LLC
Cleveland, Ohio 44135

Abstract

In October 2022, the Lunar LTE Studies (LunarLiTES) team from the National Aeronautics and Space Administration (NASA) Glenn Research Center (GRC) conducted a series of communications field test measurements through the NASA Desert Research and Technology Studies (DRATS) campaign held near Flagstaff, Arizona [1]. The objective of the NASA DRATS outings are to provide analog mission testing of candidate technologies for space exploration, especially those technologies applicable to human exploration of extraterrestrial rocky bodies. These activities are performed at locations with similarities to extraterrestrial conditions, such as the dry, volcanic landscape north of Flagstaff. This report describes the surface-to-surface communications testing performed by LunarLiTES as part of the 2022 NASA DRATS experiments. The objectives of this testing were to collect data for the development and refinement of radio frequency (RF) propagation models and emulation techniques, as well as to evaluate the application of terrestrial cellular communication technologies to lunar surface exploration.

Contents

I Introduction 3

II Methodology 3
- II-A Test Sites . . . 3
- II-B Models . . . 5
  - II-B1 SPLAT! Model . . . 6
  - II-B2 MATLAB Longley-Rice Model . . . 6
  - II-B3 Analytic Propagation Approximation Model . . . 7
- II-C Testbed Description . . . 7

III Results and Discussion 9
- III-A Results . . . 9
- III-B Discussion . . . 11

IV Conclusion 13

References 14

Appendix 16
- A Software . . . 16
- B Test Summary . . . 19

List of Tables

I Model simulation parameters . . . 5
II Radio configuration settings . . . 9
III Summary of conducted field tests . . . 19

List of Figures

1 Test-subjects conducting field tests with a view of the lava-flow terrain near SP Crater. . . . 3
2 Test location map . . . 4
3 Test location terrain . . . 5
4 SPLAT! model results . . . 6
5 MATLAB Longley-Rice model results . . . 8
6 Analytic Propagation Approximation model results . . . 8
7 Communications topology for lunar analog testing. . . . 9
8 Testbed nodes as deployed for field experiments . . . 10
9 Signal strength measurement results . . . 10
10 Comparison of Longley-Rice model to measured data . . . 12
11 Comparison of the APA model to measured data . . . 12
12 Imagery of terrain at locations where future model refinement is necessary. . . . 13
13 Representative spectrogram measurement results. . . . 14
14 Software user interface web pages . . . 17
15 Example software pages during a field test depicting a loss of communications event . . . 18

I. Introduction

Studies are ongoing to develop the lunar surface network architecture that will support the exploration goals of NASA's Artemis program. The legacy UHF Space-to-Space Communication System (SSCS), long used for critical voice communications on the Space Shuttle and International Space Station (ISS), is not expected to meet long-term needs for lunar surface operations, primarily due to its limitations in telemetry data rate and total number of users. In addition, communication system designs for mostly free-space point-to-point links, such as on ISS and Shuttle, are considerably different than those for communication over variable terrain with antennas located near the surface. Terrestrial communications standards, including cellular 4G/5G/6G and WiFi-5/6, are thus being evaluated as potential technologies to support the overall lunar communications architecture. In addition to their technical capabilities, use of these terrestrial standards also leverages the significant investment in their development for terrestrial use as well as their inherent standardization and interoperability. In support of developing modeling capabilities for lunar surface communication, and to provide recommendations for the lunar surface communications system design, field experiments were conducted near Flagstaff, Arizona. The goal of the conducted experiments was to collect measurements for radio frequency (RF) signal strength in an environment which has similar characteristics to that of exploration locations on the lunar surface. In addition to the arid environment, the test environment contains numerous terrain features and variations which are akin to the lunar surface. Figure 1 shows various terrain features at the field location, which includes for example arid open plains, buttes and hills, as well as a volcanic lava field. The objective was to collect measurements at locations that would verify current models as well as at locations where it was expected that current state-of-practice RF propagation models would likely deviate from real-world observations. Thus, measurements were collected at locations where it was expected that the simulation models would likely not match the measurements. This work compares the measurements with standard propagation models, such as the Longley-Rice Irregular Terrain Model (ITM) [2], to determine locations where the existing models may fail. Yet the intent of this work is not to directly evaluate the propagation models used. Rather, the results of these measurements will be used in future work, which will utilize these measurements in support of RF channel emulation model development. This document provides a description of the methodology used to perform the measurements, including an overview of the RF propagation models used and the test-equipment used, followed by a comparison of the collected measurements to the software models.

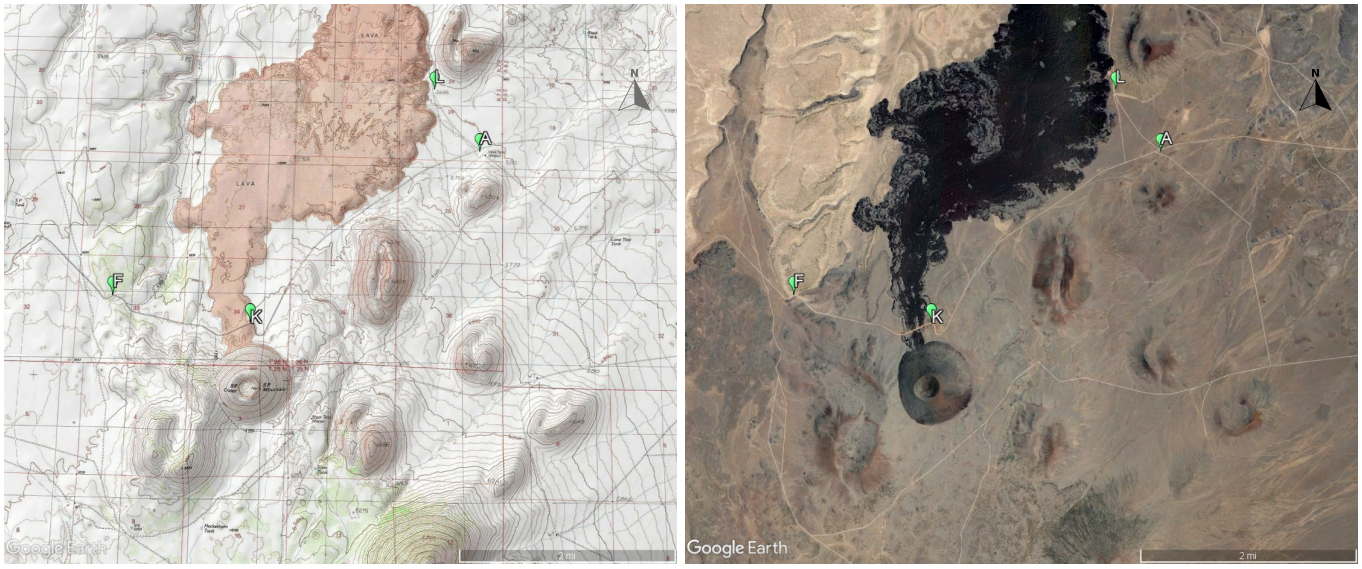
II. Methodology

A. Test Sites

The Desert Research and Technology Studies (DRATS) efforts are focused on analog mission testing of candidate technologies for space exploration, especially those technologies applicable to human exploration of extraterrestrial rocky bodies. These activities are performed at locations with similarities to extraterrestrial conditions. The 2022 DRATS activities were conducted in the desert near the San Francisco Volcanic Field, located north of Flagstaff, AZ. The RF communication efforts described in this work were conducted north of SP Crater, a cinder cone with a lava flow extending 7 km to the north [3]. National Aeronautics and Space Administration (NASA) has previously used the testing location near Flagstaff, AZ for other radio communication tests to develop communication methods in preparation for lunar surface operations [4]. The terrain provides an opportunity to test RF communication links in an environment that is, at least in some capacity, similar to that of the lunar surface. While the environment still



Fig. 1: Test-subjects conducting field tests with a view of the lava-flow terrain near SP Crater.



(a) Topographic Map. Map Source [5].

(b) Satellite Imagery. Map Source [6].

Fig. 2: Test locations depicted on topographic map with corresponding satellite imagery of the testing area.

differs in a number of ways (such as the presence of an atmosphere, the larger radius of curvature of the Earth, and higher moisture content in desert soil than in Lunar regolith), it does also offer a reasonable test analogue considering the sparse vegetation, similar rocky and cratered topography, and relative dryness as compared to other terrestrial locations. Specific testing sites in the region were selected based on the basic criteria of a) accessibility, b) variability of the terrain and its RF characteristics, and c) availability:

a) Accessibility: The terrain must be accessible by vehicle to transport equipment and to perform tests using a vehicle, thereby increasing the total available testing area. In addition, the regions which where easily accessible by vehicle should have options to collect data on multiple vehicle paths/routes near a location where a base-station tower could be deployed. A favorable base-station location would also provide coverage of multiple roads and intersections for multiple traverse path options by vehicle.

b) Variability: The selection of the site is based on the variability of the terrain present. The site must have terrain of interest, with the opportunity to test in locations with various RF propagation characteristics. For example, the testing regions selected include an open plains region, where it is expected that RF propagation models will most accurately predict in-situ results. In addition, terrain near-by was available where it is expected that measured results would deviate from simplified RF path-loss models.

c) Availability: The selected test region must be available for on-site presence, with permission to deploy equipment and operate with agreements in place with the land owners. In addition, the region must also have sufficient RF coverage from a deployed base-station to conduct the tests.

To aid in the test-location selection, initial RF path-loss calculations were performed using the Longley-Rice Irregular Terrain computation method [2]. Details of the modeling software used to determine the RF propagation characteristics for test-site locations is discussed in Section II-B1. Numerous potential test-sites were evaluated, with the selection of the following four locations: 1) Site A: Open Plains, 2) Site L: Canyon, 3) Site F: West of Lava Flow and 4) Site K: East of Lava Flow; where each site is labeled with the corresponding terrain feature of interest. A map depicting the selected locations is found in Figure 2.

Site A, the open plains region, was selected due to the flat terrain. On-site measurement results are expected to match the simulation models, as the terrain features are slowly varying with continuous line of sight between a stationary base-station and a mobile node deployed in the region. As a result, minimal multi-path characteristics are expected. Thus, the measurement results are expected to provide initial verification of the path-loss models.

Site L, the canyon region, was selected due to the narrowing and rising terrain. One side of the canyon is bordered by the lava flow to the north of SP Crater. The canyon environment is expected to exhibit multi-path effects. Entry into the canyon region is made from the open plains region and the surrounding terrain has slopes that may be traversed on foot, allowing for measurements at elevations above the deployed base-station tower.

Site F and K, located on the west and east sides of the lava flow respectively, were selected due to the close proximity of the lava flow. The location is easily accessible by vehicle. A well-established dirt road runs across the lava flow near the base of SP Crater, allowing for RF measurements to be collected at locations within the lava flow by vehicle. In addition, the terrain adjacent to the flow is a flat plains area, allowing one to easily traverse along the edge of the lava



(a) Site A: Open Plains

(b) Site L: Canyon

(c) Site F: West of Lava Flow

(d) Site K: East of Lava Flow

Fig. 3: Test location terrain view as observed from the base station tower locations.

Parameter	Value
Earth Dielectric Constant	6.7
Earth Conductivity	0.005 [S/m]
Earth Loss Tangent	0.0147
Atmospheric Refractivity	256.3 [N-Units]
Frequency	915 MHz
Radio Climate	Continental Temperate
Polarization	Vertical
ITM Fraction of Situations	0.5
ITM Fraction of Time	0.9
Effective Radiated Power (ERP)	1 W

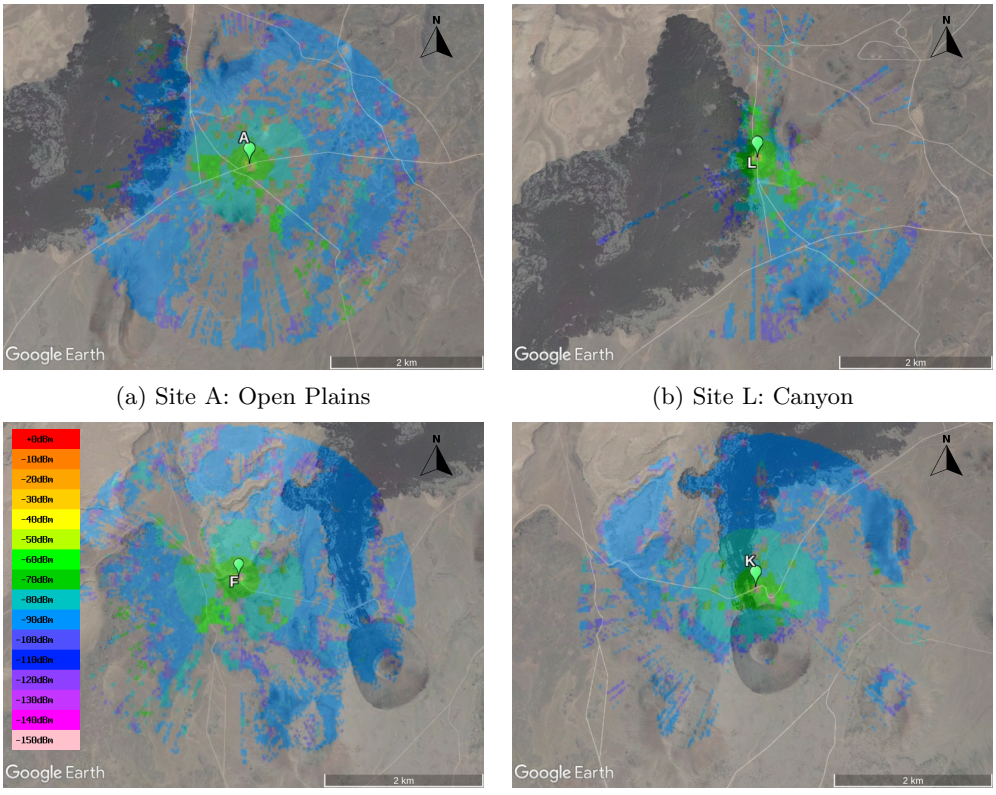
TABLE I: Model simulation parameters

flow by foot. The base-station tower is positioned such that one can transition into and through the lava terrain to the other side while making measurements. The lava flow environment is expected to exhibit multi-path effects, including both diffraction and scattering.

Figure 3 shows an on-site view from each of the selected test locations. It should be noted that each of these locations were selected based on the local terrain. The intent was to collect measurements in regions where RF communication was expected to be challenging. The locations would not necessarily be selected if one were trying to maximize communications coverage for the region.

B. Models

RF propagation models were used in preparation for the field-tests, as well as for analysis of the collected measurement data. Standard propagation models using the Longley-Rice ITM methods were used to aid in the site selection and to provide initial predictions on RF connectivity. The parameters used for the model simulations are found in Table I. The electrical characteristics of the Earth were calculated using the ITU-R P.527 recommendation [7]. Soil properties for the testing area necessary for calculating the electrical characteristics of the Earth were obtained from the United States Department of Agriculture (USDA) Web Soil Survey online tool [8]. The soil was primarily a very cindery loam type (Wukoki Series / Wupatki Series), consisting of approximately 78 % sand and 16 % silt. The radio refractive index was calculated using local measurements for the atmospheric pressure and temperature and the ITU-R P.453 recommendation [9]. In preparation for the field-tests, the open source software tool Signal Propagation, Loss, And Terrain (SPLAT!) [10] was used to evaluate potential sites. After completion of the field tests, two different models were used for comparison of the measured RF signal strength data to model results. The first model used is the MATLAB communications toolbox, a commercially available software package. The SPLAT! and MATLAB software programs both use Longley-Rice models for computations and as such the results are expected to be similar. The other analysis method was constructed using information as published in the open literature by Chizhik et al. [11], [12]. The



(a) Site A: Open Plains

(b) Site L: Canyon

(c) Site F: West of Lava Flow

(d) Site K: East of Lava Flow

Fig. 4: SPLAT! path loss model results performed prior to testing using desired tower locations. Results are depicted for 2.5 km radius around the base tower. Geometry assumes a 10 m tall base tower with the mobile antenna located at 2 m above the surface. Map source: [6].

Analytic Propagation Approximation (APA) model by Chizhik et al. does not use a Longley-Rice modeling technique and is provided in this work as an alternative. The motivation here is not for model comparisons, but rather simply to present an alternative modeling approach. Ultimately, the goal of this work is to contribute to the development of a robust emulation environment wherein multiple models can be deployed according to their known strengths and weaknesses. For example, some models may better characterize diffraction while others more accurately predict delay spread. The test sites were therefore chosen to stress the models, as noted above, not with the goal of finding one optimal and generalized model, but to discern the best use cases for different models and vice versa. These results will help to provide information regarding potential differences in results when attempting to apply the models to the lunar surface environment. It should be noted, that the APA model was reconstructed herein only from available information in open literature, and thus one can not be certain that the implementation of the model as deployed here is entirely complete.

1) SPLAT! Model: The open source software tool Signal Propagation, Loss, And Terrain (SPLAT!), is an RF propagation and terrain analysis tool for terrestrial applications [10]. SPLAT! uses the ITM for computing path attenuation and received signal strength for the spectrum between 20 MHz and 20 GHz. According to the author [10], the tool computes "path loss and field strength based on the Longley-Rice Irregular Terrain as well as the new Irregular Terrain With Obstructions Model (ITWOM v3.0)". Terrain information is included in the model by using the Shuttle Radar Topography Mission (SRTM) [13] Digital Elevation Model (DEM) available from the United States Geological Survey (USGS). The 1 arc-second data from the SRTM-1 Version 3 Elevation models are used for the calculations in this work. Using the software, the path loss analysis could be performed quickly, with low computational complexity, to generate path loss and signal strength contours. RF coverage predictions at potential tower sites were generated to assist in the site selection process. The ITM parameters used for the model are found in Table I and the model results are found in Figure 4.

2) MATLAB Longley-Rice Model: The MATLAB software available from Mathworks Inc. provides several tools for RF analysis [14]. One available toolbox is the Communications Toolbox™ [15]. By using built-in map data and propagation parameters, MATLAB is able to estimate the propagation characteristics. SiteViewer is a component of the Communications Toolbox™ that allows the user to visualize built-in models such as the Longley-Rice and

free-space path-loss models [16]. Here, the Longley-Rice model is used for comparison to the measured RF signal strengths. The simulation domain is limited by the available memory of the computer used for the analysis, which in this work restricted the maximum distance from the transmit tower to about 6 km or less depending on the model parameters selected. By default, analyses which include terrain are limited to a resolution of 30 meters, or 1 arc-second. By defining antenna parameters, such as antenna type, antenna height, frequency and power, MATLAB can generate a coverage map. Additional parameters from the Antenna Toolbox™ may also be set to further configure specific antenna characteristics [17] but were not used in these results. The estimation results for the field-test locations as specified in Section II-A are depicted in Figure 5 using the Longley-Rice model using the parameters listed in Table I with a 1 arc-second terrain and an isotropic antenna.

3) Analytic Propagation Approximation Model: Chizhik et al., [11], [12], developed a simple and effective way to calculate propagation over variable terrain. The APA model utilizes Green's Function and parabolic analysis to calculate the received power at a given location. By repeating the process using a DEM file, a 3D prediction of the propagation can be calculated. The accuracy of the model is dependent on the DEM resolution used and variations in the terrain which are smaller than the resolution of the DEM will not be captured in the model results. The APA Model does not take into consideration soil permittivity or the effects due to the presence of vegetation. The model only takes the propagation frequency, transmit location and terrain as input parameters. Figure 6 depicts the simulation results for the field-test locations as specified in Section II-A by using 1/3 arc-second DEM files from USGS. The results were visualized using the MATLAB SiteViewer software for consistency with the depiction of the MATLAB Longley-Rice model results.

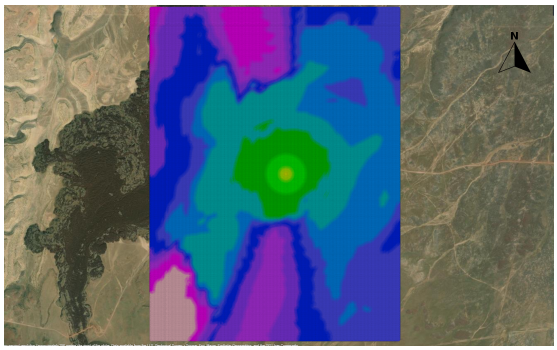
C. Testbed Description

In support of the field test experiments, a communications testbed was constructed. A hypothetical lunar communications scenario was conceived and then represented using a notional communications topology. It is assumed for simplicity here that all elements may communicate with each other via an IP-addressable communications network. An illustration of the test topology is depicted in Figure 7. The test setup consists of a stationary communications terminal (base station tower) connected to a ground station terminal. Additional mobile or stationary users are connected to the stationary communications terminal via an Industrial, Science and Medical (ISM) band radio; the ISM band was used here only due to available spectrum and laboratory hardware and is not reflective of ultimate lunar communications architecture spectrum. A mobile communications node is used to represent either an Extravehicular Activity (EVA) crew member or a lunar rover. During the conducted field tests, only one mobile node was operational at a given time. A stationary user node was used to represent a deployed asset, such as a science terminal or a habitat module. For the purposes of the field test, the stationary node is used as a cross-check to verify system functionality during the experiment, as the RF environment between the base station tower and that stationary node will remain consistent throughout the test, whereas the mobile node will clearly be subjected to dynamically changing terrain between the two elements.

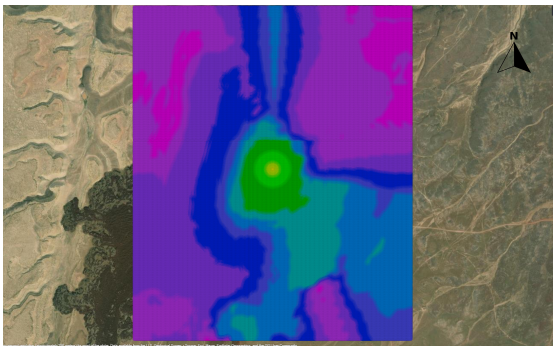
The hardware used to construct the communication nodes consists of Commercial Off-The-Shelf (COTS) hardware. All of the nodes share the same foundational elements for hardware and software. The common set of hardware includes an i686-based General Purpose Processor (GPP), an ISM band (900 MHz) Orthogonal Frequency-Division Multiplexing (OFDM) radio, and a Global Positioning System (GPS) receiver. Additional hardware and software elements are added to address specific needs of the node. For example, the mobile node contains a digital magnetometer for attitude information in addition to a web camera for informational images. The stationary user terminal includes a weather station terminal for simulated science data and for monitoring environmental conditions for future use in further model refinement.

The GPP is paired with a Debian Linux distribution to aid in the rapid prototyping by leveraging the inherent support for development software and hardware drivers. The GPP runs the entire networking stack, handles the interfaces for all of the other hardware components and processes all incoming and outgoing data. The GPS unit, connected via serial port to the GPP, generates position information once per second. The location is transmitted over the active RF interface back to the base station to allow for monitoring the test status.

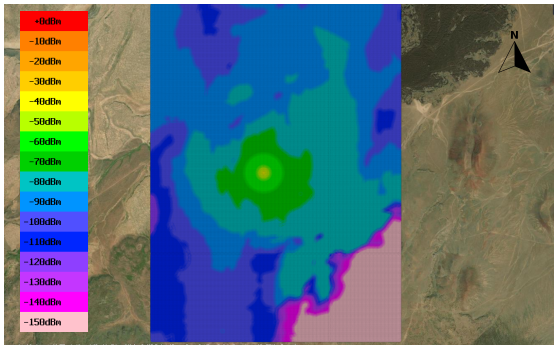
An outdoor Access Point (AP)-class ISM band (900 MHz) OFDM radio is selected as the communications interface and is paired with dipole antennas. The ISM band was selected primarily due to hardware availability as well as to preclude any issues associated with spectrum usage authorization for the field tests. An OFDM radio was selected because of the favorable propagation characteristics including mitigation of multi-path fading. In addition, OFDM is used in terrestrial communications, including cellular 4G/LTE and WiFi-6, both of which may be potential technologies included as part of an eventual overall lunar surface communications implementation. To mitigate the effects of multipath and inter-symbol interference, OFDM is used with a 20 MHz bandwidth. Since the signal is spread out over a 20 MHz bandwidth, it is less susceptible to narrowband fading. A complete listing of all the selected configuration settings for the radio are summarized in Table II.



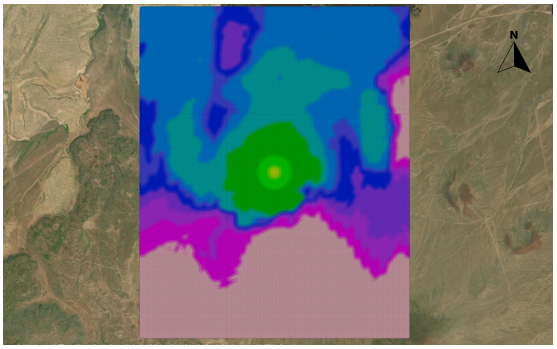
(a) Site A: Open Plains



(b) Site L: Canyon

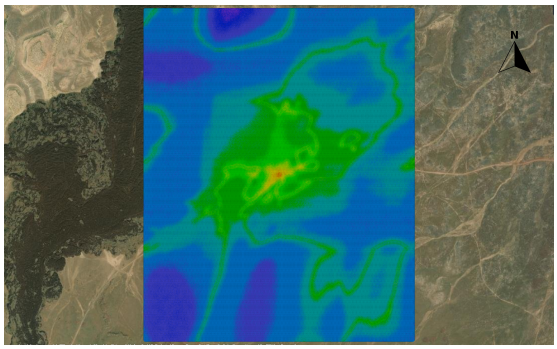


(c) Site F: West of Lava Flow

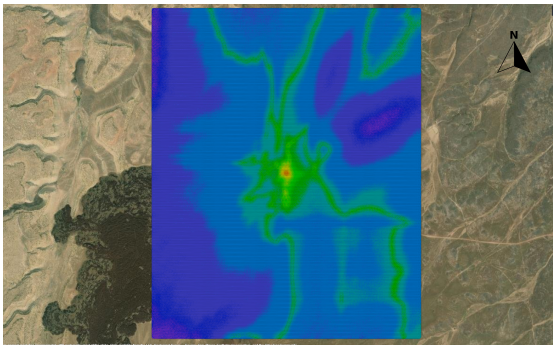


(d) Site K: East of Lava Flow

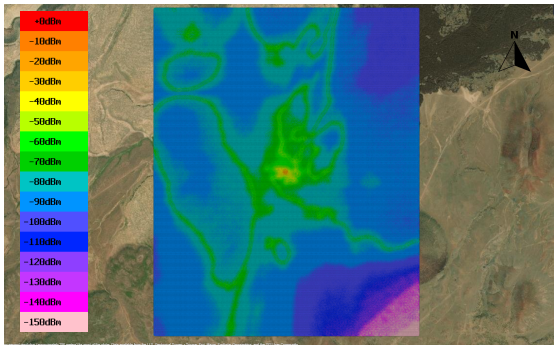
Fig. 5: MATLAB Longley-Rice model results. Map source: [18]



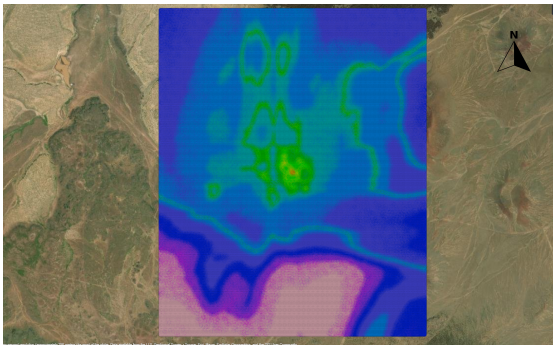
(a) Site A: Open Plains



(b) Site L: Canyon



(c) Site F: West of Lava Flow



(d) Site K: East of Lava Flow

Fig. 6: Analytic Propagation Approximation model results. Map source: [18]

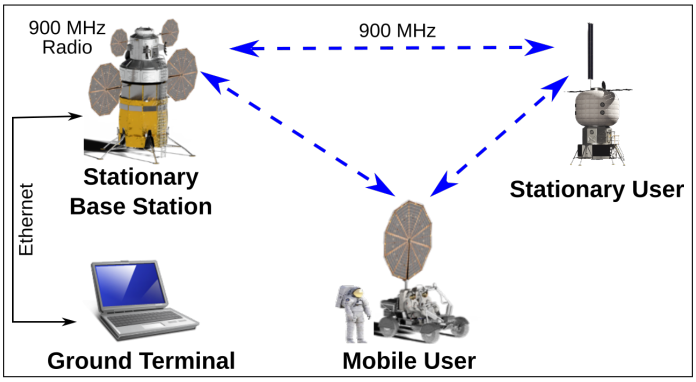


Fig. 7: Communications topology for lunar analog testing.

Configuration	Setting
Transmit Power	30 dBm
Frequency	913 MHz
Bandwidth	20 MHz
Modulation	QPSK w/ OFDM
Data Rate	6 Mbps
Fragmentation Threshold	512 Bytes

TABLE II: Radio configuration settings

All of the hardware components are enclosed in a plastic, weather resistant container for the stationary nodes. For the mobile node, the components are fixed to a plastic backing plate, which is then securely mounted to a rigid external-frame backpack via aluminum struts. Plastic masts for the radio antennas are also fixed to the plate so that the antennas can be mounted safely above the test-subject's head. The mobile node utilizes the same hardware for deployment on either the person or the vehicle. The backpack containing the hardware is placed inside a vehicle, with a coax cable run outside the vehicle to an antenna mounted on an aluminum plate located on the vehicle's roof. An aluminum plate is used to ensure a consistent ground plane for modelling purposes, as the vehicle used for the tests had a glass sunroof. Figure 8 shows the constructed testbed hardware nodes as deployed in the field during test operations.

III. Results and Discussion

A. Results

Using the communications testbed described in Section II-C, field-measured received signal strength was recorded as a function of geographic location. The values were obtained via a simple network management protocol (SNMP) interface to the radio hardware. The signal strength values are as reported by the radio hardware and are the result of unknown internal processing algorithms. The measurement values as a function of geographic location for each of the test sites described in Section II-A are depicted in Figure 9. The stationary node location is depicted with a red and black dot in each of the sub-figures. The depicted results include data collected using both the person and vehicle mobile nodes. Path segments which appear smooth and straight-line correspond to data collected using the vehicular mobile node. Since the vehicle was operated only on established gravel roads, the the path generally follows gradual changes in elevation and direction. The backpack-mounted hardware allowed the person to traverse along more rugged terrain, including ascending hills and the edge of the lava flow.

Using the field-measured signal strength as a function of geographic location, it is desired to compare the measurement values to the modeled values. For comparison purposes, a simple difference is computed where the modeled value is subtracted from the measured value (Δ = [Measured - Model]). Due to limitations of the radio hardware, the measured results are limited to above -92 dB. Therefore, any value in the model that is less than or equal to -92 dB is not included. For consistency between the model comparisons, the axes limits are set to $\pm$50 dB for the depicted results. The observed difference between the measured value and modeled value did not exceed these bounds for the model in any of the test cases.

The experimental setup utilized an omni-directional sleeve dipole antenna, which exhibits a toroidal radiation pattern. As a result, a dead zone is located directly underneath the transmitting base-station tower antenna. Thus, when calculating the difference between the measured value and the modeled values, the results for the first 20 m surrounding the base station are excluded. In this analysis, neither model takes into account the antenna pattern. While the default antenna patterns used in the models are omni-directional in azimuth, the radiation pattern is not modeled with a



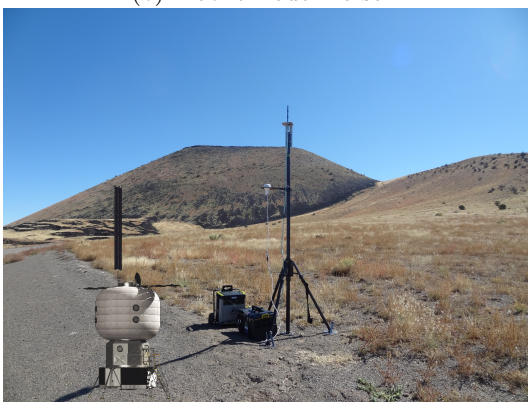
(a) Mobile Node: Vehicle



(b) Mobile Node: Person



(c) Stationary Node: Base Station

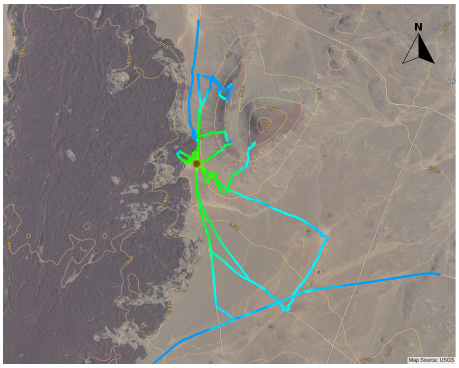


(d) Stationary Node: User Terminal

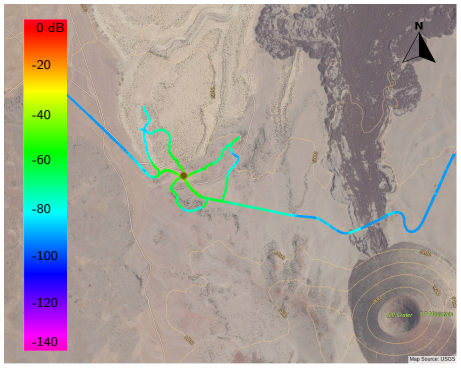
Fig. 8: Testbed nodes as deployed for field experiments. Image insets depict artist renditions of equivalent lunar assets.



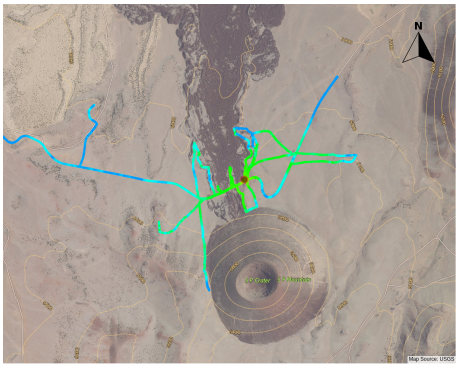
(a) Site A: Open Plains



(b) Site L: Canyon



(c) Site F: West of Lava Flow



(d) Site K: East of Lava Flow

Fig. 9: Signal strength measurement results. Map source: [19].

variation due to elevation angle. Future work will include the incorporation of the antenna radiation pattern. For the analysis presented here, one would expect to notice variations between the modeled and measured data for differences in elevation and for locations near to the transmitter tower due to the omni-directional dipole antenna radiation pattern.

Figure 10 and Figure 11 show the difference between the model and the field-measured data at each of the four test sites for the Longley-Rice and APA model respectively. Note that the attitude of the antenna was not corrected for in the raw measurement data. Tip and tilt of the antenna would have some affect on the observed received signal strength measurements. The reduced signal gain due to changes in orientation would need to be accounted for in order to directly compare the measured values with the model outputs.

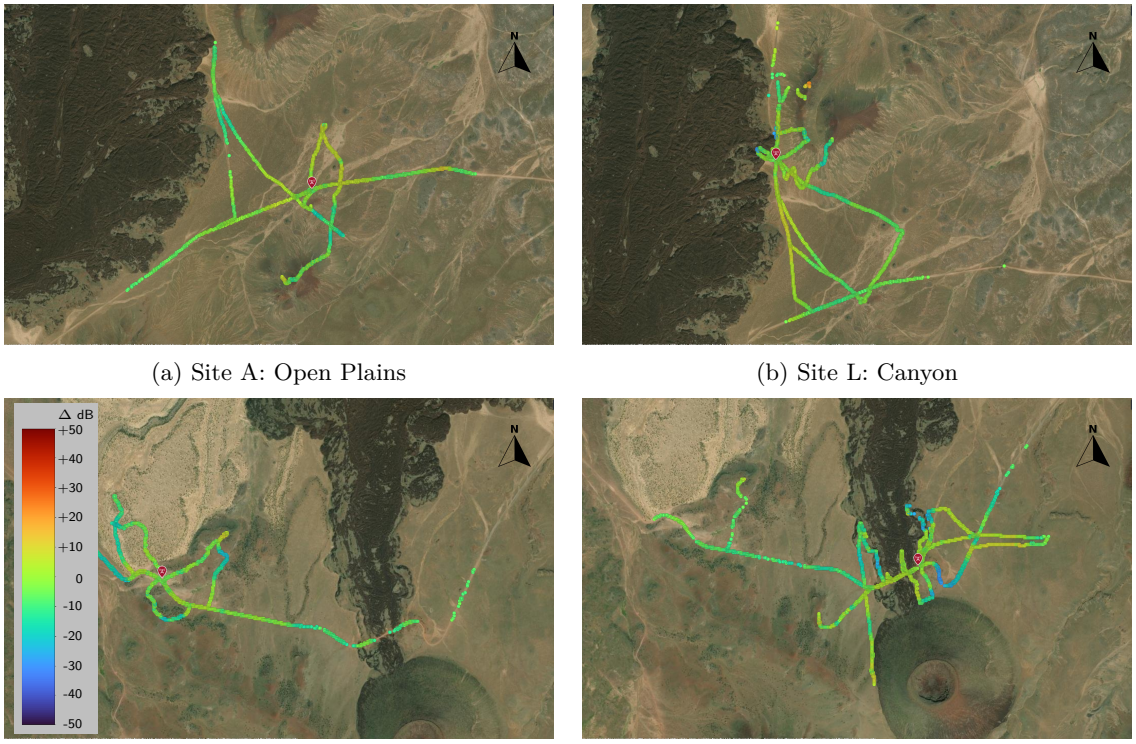
B. Discussion

It is expected that no model will represent the propagation environment in the entire region perfectly. Model limitations and the uncertainty in model input parameters contribute to the agreement of the model to any measured data. Regardless, the motivation here is to gain an understanding of the characteristics and limitations of the modeling approach such that the models may be properly applied to other environments where in-situ measurements are not readily available. The models used in this work are limited by the resolution of the terrain data and do not completely represent multipath effects. Comparison of the measured signal strength to the model values indicates geographical locations where these limitations are encountered. Figure 12 shows representative images at locations in the field where anomalies were observed. Figure 12b show an example of a terrain feature which was not included in the terrain map. The depicted rock outcropping is approximately 3 to 4 m tall, resulting in a shadowed signal over 25 dB, yet was too small to show up on terrain digital elevation map of 1/3 arc second, (10 m). The resolution of the digital elevation map information will limit the accuracy of the model results.

Figure 12d shows a representative image of the lava flow, where data was collected on foot with the mobile node. Due to the terrain, traversing into the lava flow was limited. During testing, the test subject traversed up and into the lava flow well beyond line-of-sight but were able to maintain signal for longer than predicted by the models. The observed behavior may indicate a need to adjust the propagation model parameters for characteristics of the lava rock terrain. Lava rock is an uncommon medium for radio propagation modeling and therefore the model propagation parameters for the terrain had to be estimated.

Figure 12a depicts the canyon region near Site L, where one side of the path is bordered by the lava flow and the other side by rising terrain. During testing, the vehicular mobile node was driving north through the canyon and observed an initial loss of signal as expected. After continuing the direction of travel along the gravel road, the received signal level did not return to the values predicted by the model, even in conditions with clear line-of-sight. This observation may be indicative of strong multipath fading conditions. Inspection of the measured results as compared to the modeled values, confirms the expected multipath behavior. Consider for example the results for test Site A as depicted in Figure 10a for the Longley-Rice model. In this case, the data collected at the northern region follows an established gravel road that runs parallel and below the lava flow (depicted by the dark terrain). Multipath effects would be expected in this region due to the lava flow, which rises above the route. Figure 10a clearly shows a deviation from the measured data in this region, with the modeled value greater than the actual measured value. Inspection of the results for the APA model, Figure 11a, shows a similar deviation from the measured results in this region.

Neither model used in this work utilizes ray-tracing techniques and therefore multipath propagation characteristics are not fully represented by the model results. The Longley-Rice model does account for some diffraction attenuation, such as knife edge diffraction, but does not model fast-fading multipath effects. The 'Time Variability' parameter indicates long-term signal variability, but short term variability associated with fast multipath fading is not included. The 'Canyon' test region may be particularly difficult to model, as one side is bounded by the lava flow, which is not only at a higher elevation, but would contribute to multipath effects due to the the rough, irregular terrain. Site L had the base station tower located near to the lava flow in comparison to other test sites. At this location, one would expect to have a stronger multipath signal as compared to Site A for example, where the tower is located farther away from the lava flow. During the experiments, RF spectrum information was recorded at the stationary base station node using a Keysight FieldFox portable RF analyzer. Spectrum information as measured by the RF analyzer was recorded in snapshots at approximately ten-second intervals. Spectrum measurements from one experimental test at each test site were assembled into spectrograms as shown in Figure 13. While the radio is not transmitting RF energy continuously, the portions of the spectrogram where the radio is transmitting RF energy lends insight. When the radio is emitting RF energy, one would expect to observe in the spetrogram energy across the entire bandwidth occupied by all of the OFDM sub-carriers, around the center frequency, (913 MHz, Table II). Multipath flat fading, or where the sub-carrier signals experience similar levels of fading, may occur yet the signal level is similar across the band. Inspection of Figure 13a for Site A shows the energy distributed across frequency, whereas Figure 13b depicts gaps in the signal as a function of frequency, indicating multipath effects with frequency selective fading. The spectrogram also depicts numerous gaps along the time axis. While the radio used is not transmitting continuously, the number of observed



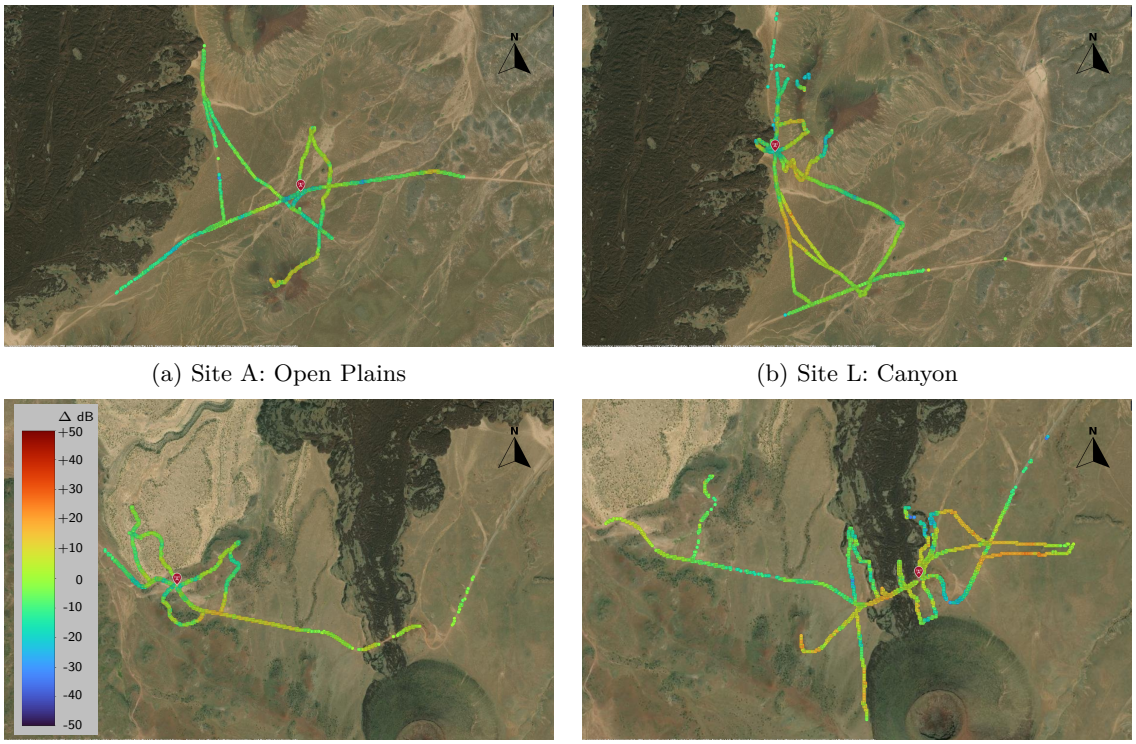
(a) Site A: Open Plains

(b) Site L: Canyon

(c) Site F: West of Lava Flow

(d) Site K: East of Lava Flow

Fig. 10: Comparison of Longley-Rice model results to measured data. Results depict the difference between the measured data and the model values, Δ = [Measured - Model]. Map source: [18].



(a) Site A: Open Plains

(b) Site L: Canyon

(c) Site F: West of Lava Flow

(d) Site K: East of Lava Flow

Fig. 11: Comparison of the APA model results to measured data. Results depict the difference between the measured data and the model values, Δ = [Measured - Model]. Map source: [18].



(a) Canyon



(b) Rock Outcropping



(c) Lava Rock Hill



(d) Lava Flow

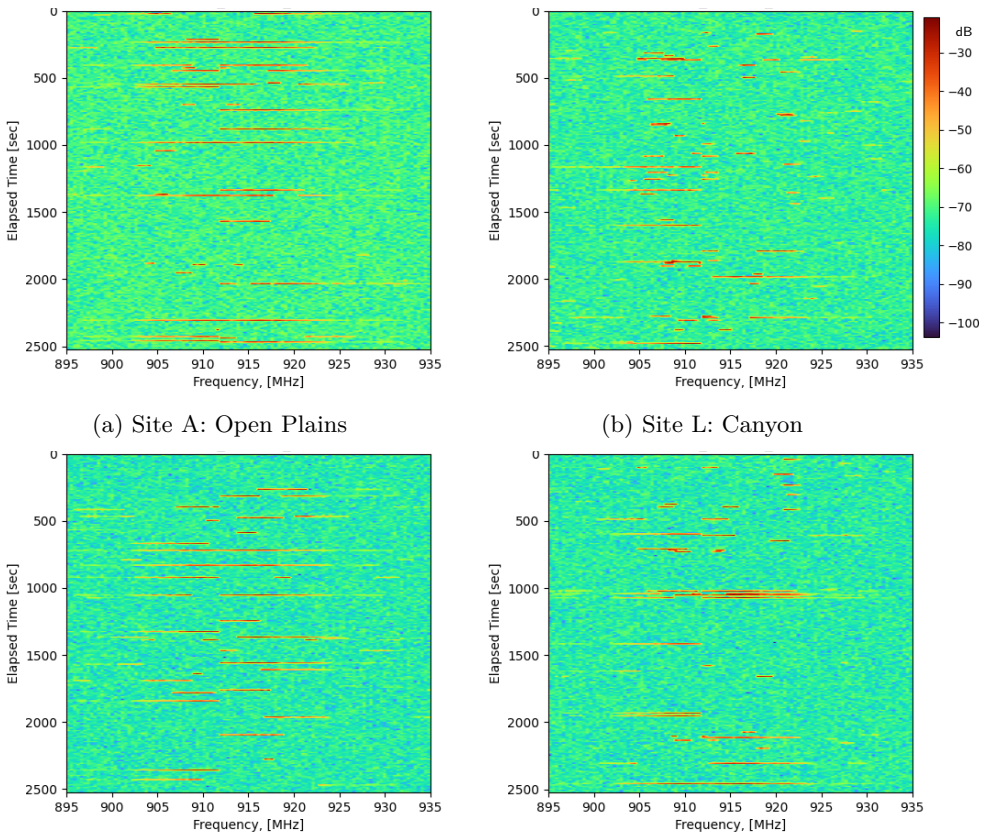
Fig. 12: Imagery of terrain at locations where future model refinement is necessary.

loss of signal events suggests the possible existence of multi-path flat fading across the 20 MHz bandwidth. Given the measurement methods of the test, it is difficult to distinguish between a loss of signal event due to terrain obstructions versus multipath flat fading effects. Regardless, inspection of the data indicates that the multipath conditions at the testing area likely had a greater influence than predicted and perhaps an OFDM bandwidth greater than 20 MHz is necessary in this environment. Future work may include both ray-trace modeling and on-site measurements to measure the multipath environment delay spread statistics. The deviations of the measured data from the model values for Site L near the lava flow and the stationary base station as shown in Figure 10b and 11b are likely due to the multipath environment. At locations near the stationary base station and near the lava flow at Site L, the APA model was less than the measured values whereas the Longley-Rice model was greater than the measured values.

Any model is only as good as the confidence in the input parameters. It is important to note that the APA Model only uses the transmit frequency and terrain as input parameters and does not take into account the soil permittivity, whereas the Longley-Rice model does take into account the soil electrical characteristics. The soil electrical characteristics were estimated using typical soil properties of the region. The region included multiple soil types and the soil water content was not measured on-site. The field tests were interrupted for one test day due to a precipitation event (Oct. 16, 2022. Refer to the test summary, Table III). Since the soil characteristics are estimated based on typical conditions, it is likely that better estimates of the actual conditions would bring the Longley-Rice model towards agreement with the measurements.

IV. Conclusion

Surface-to-surface communications field test measurements were collected near Flagstaff, AZ where various terrain features provide a rough analog to the RF propagation characteristics of the lunar surface. The primary motivation of this effort was to accumulate a robust set of field test data that will be used in the development and validation of simulation and emulation tools for lunar surface communications architectures. The RF signal strength measurements were compared to traditional Longley-Rice propagation models [2], as well as an Analytic Propagation Approximation (APA) model found in the literature from Chizhik et al. [11], [12]. The APA model is of interest for potential application to the lunar environment, since the model does not utilize information about the soil permittivity. Such a model may be useful in situations where permittivity parameters are either unknown, not known to a high-level of certainty, or where values may be variable over the test region. While the model accuracy for the Longley-Rice model may improve with refinement of the input parameters, the current results indicate the Longley-Rice model was consistent with the measurements with a tendency to over-predict the performance resulting in an optimistic performance estimate.



(a) Site A: Open Plains

(b) Site L: Canyon

(c) Site F: West of Lava Flow

(d) Site K: East of Lava Flow

Fig. 13: Representative spectrogram measurement results.

In comparison, the APA model results tend to under-predict the performance resulting in a positive margin and a conservative estimate. The difference is likely directly related to the soil permittivity parameters, which were estimated using typical characteristics for the soil found in the test region. While multipath conditions were expected in the test region due to the terrain, it was expected that the OFDM signal waveform would overcome the effects, as the OFDM signal by design eliminates or reduces frequency selective fading effects. Yet, the multipath effects were greater than expected, indicating that the conditions may necessitate a wider OFDM bandwidth, a potential future consideration for trade studies of 4G versus 5G, given the increase in the maximum channel bandwidth from the former to the latter.

References

[1] NASA, "Desert Research and Technology Studies (Desert RATS)," Online. Accessed January 2023. https://www.nasa.gov/hrp/research/analogs/drats.

[2] Longley, A. G., *Prediction of tropospheric radio transmission loss over irregular terrain: A computer method-1968*, Vol. 67, Institute for Telecommunication Sciences, 1968.

[3] U.S. Geological Survey, "San Francisco Volcanic Field, Geology and History," Online, Accessed January 2023. https://www.usgs.gov/volcanoes/san-francisco-volcanic-field/geology-and-history.

[4] Swank, A. J. and Bakula, C. J., "EVA radio DRATS 2011 report," 2012, NASA/TM-2012-217635.

[5] U.S. Geological Survey, "USGS Topo Maps, National Geographic Society, i-cubed," Online, Accessed January 2023. https://services.arcgisonline.com/arcgis/rest/services/USA_Topo_Maps/MapServer.

[6] Google Earth Pro, 7.3.6.9345, "May 23, 2021. SP Crater, AZ. 35°35'50.25" N, 111°37'05.12" W, Eye alt 34457 ft," Accessed January 2023.

[7] International Telecommunication Union: Radiocommunication, *Recommendation ITU-R P.527-6: Electrical characteristics of the surface of the Earth*, 2021.

[8] U.S. Department of Agriculture, "Web soil survey, Natural resources conservation service," USDA Soil Survey: Coconino County Area, AZ, Central Part (AZ631). Online, Accessed June 2023. https://websoilsurvey.nrcs.usda.gov/app.

[9] International Telecommunication Union: Radiocommunication, *Recommendation ITU-R P.453-11: The radio refractive index: its formula and refractivity data*, 2015.

[10] Magliacane, J., "SPLAT!, RF Signal Propagation, Loss, And Terrain analysis tool," Online. Accessed January 2023. https://www.qsl.net/kd2bd/splat.html.

[11] Chizhik, D., Drabeck, L., and MacDonald, W. M., "Propagation Over Parabolic Terrain: Asymptotics and Comparison to Data," *IEEE Transactions on Antennas and Propagation*, Vol. 58, No. 6, 2010, pp. 2012–2020.

[12] Chizhik, D., Moilanen, J., Klein, S., Maestro, L., and Valenzuela, R. A., "Analytic Propagation Approximation over Variable Terrain and Comparison to Data," *2020 14th European Conference on Antennas and Propagation (EuCAP)*, 2020, pp. 1–3.

[13] Farr, T. G., Rosen, P. A., Caro, E., Crippen, R., Duren, R., Hensley, S., Kobrick, M., Paller, M., Rodriguez, E., Roth, L., Seal, D., Shaffer, S., Shimada, J., Umland, J., Werner, M., Oskin, M., Burbank, D., and Alsdorf, D., "The Shuttle Radar Topography Mission," *Reviews of Geophysics*, Vol. 45, No. 2, 2007.
[14] MATLAB, "RF Propagation Tools," Online. Accessed January 2023. https://www.mathworks.com/help/antenna/rf-propagation.html.
[15] MATLAB, "Communication Toolbox™," Online. Accessed January 2023 https://www.mathworks.com/products/communications.html.
[16] MATLAB, "Site Viewer," Online. Accessed January 2023. https://www.mathworks.com/help/antenna/ref/siteviewer.html.
[17] MATLAB, "Antenna Catalogue," Online. Accessed January 2023 https://www.mathworks.com/help/antenna/antenna-catalog.html.
[18] U.S. Geological Survey, "USGS GMTED2010 7.5 arc-second, Esri, Maxar, Earthstar Geographics and the GIS user community," Accessed January 2023.
[19] U.S. Geological Survey, "USGS Imagery Topo, The National Map: Orthoimagery and US Topo," Online, Accessed January 2023. https://basemap.nationalmap.gov/arcgis/rest/services/USGSImageryTopo/MapServer.

Appendix

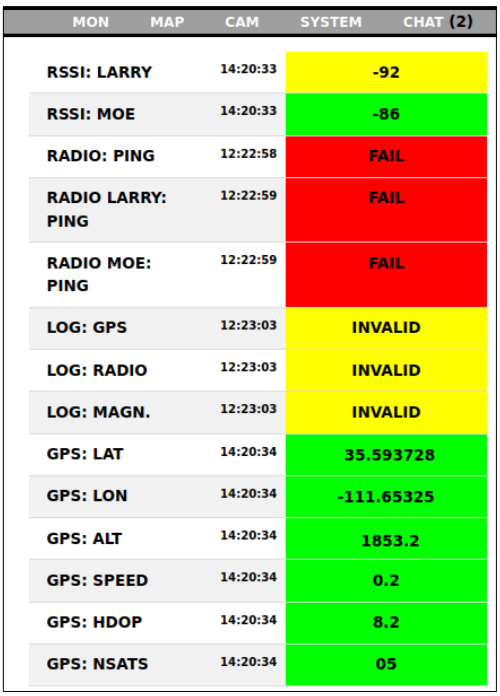
A. Software

Software to support the DRATS experiments was developed for experiment operation, data acquisition, experiment monitoring and data archival. The software may be divided into two categories, one is the user visualization and control software, and the other is functional software for system operation and data acquisition. The user visualization and control software is accessed via a web browser on a network connected device, such as a laptop computer. The main functional software for system operation is located on the GPP and is identical for each of the deployed testbed nodes.

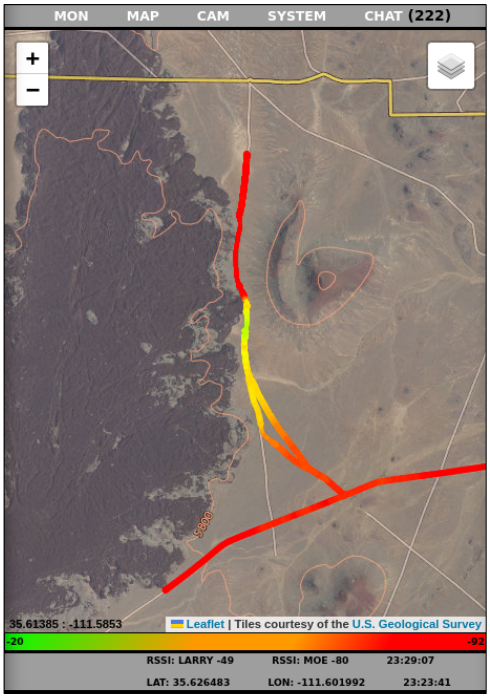
The main software application consists of an automated system status and experiment monitoring system, automated data acquisition from hardware, a command interface system and a chat messaging system. Configuration parameters are used to customize the software operation depending on which hardware and sensors are physically present. For example, only the mobile node had a web camera and magnetometer installed, and only one stationary node had the ability to record weather data. For each hardware element on the node, a separate software application is used for the sole purpose of acquiring data. The data is then stored to disk and also communicated to the main software application using a SocketIO connection. Independent software applications for each module allows the system to record data from any hardware device without concern for proper functionality of the other sub-systems. In addition, data will be recorded from each sensor regardless if the main software is listening for the information. The software is written using the Python programming language. The software applications developed include:

- Camera Acquisition: Collects and stores web camera image, sends to web application for viewing.
- Chat Application: Interface to messaging system.
- GPS Application: Records raw GPS position data from the hardware.
- Magnetometer Application: Records magnetometer attitude information.
- Monitor Application: Monitors experiment software for proper operation and proper data acquisition.
- RF Power Application: records total RF power received.
- Radio Application: records received signal strength information via SNMP interface to the radio.
- RF Spectrum Application: records RF spectrum information recorded by Keysight FieldFox device.
- Web Application: Main application that provides the web-based user interface. The application displays system monitoring information, collected data, plots radio received signal strength indicator (RSSI) data on maps, and plots RF spectrum and provides user command interface.
- Weather Application: records weather temperature and humidity data.

The user visualization and control software is used to monitor experiment status, to provide experiment operation commands while in operation and to provide text communication to field test conductor. The user visualization and control software is accessed via a web browser and consists of Python Flask application (web server application) and a web client application (HTML/javascript) for information display and human interface. The web client solution allows any device with a web browser to view and run the experiment. The web client system acts as a web-based display for the monitoring of system parameters with simple “Green, Yellow, Red” indicators with data displayed. The color indicators allows the experiment operator to quickly scan a parameter set to determine that system is operating normally. Test data is also plotted on a satellite image (map) for monitoring the experiment data during the test. Figure 14 shows example web browser system interface pages and Figure 15 shows an example of the monitor page during nominal operations when a loss of communications event occurs.



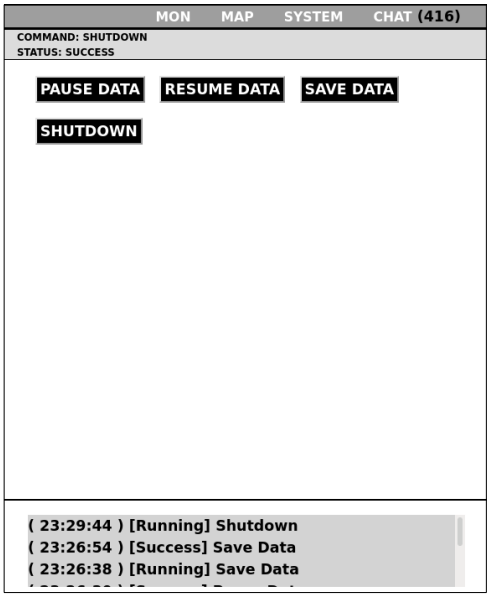
(a) Monitor



(b) Map

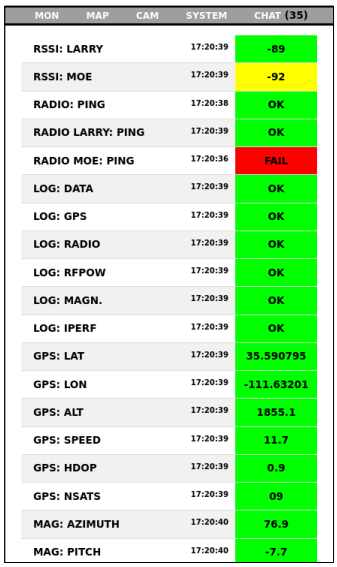


(c) Camera

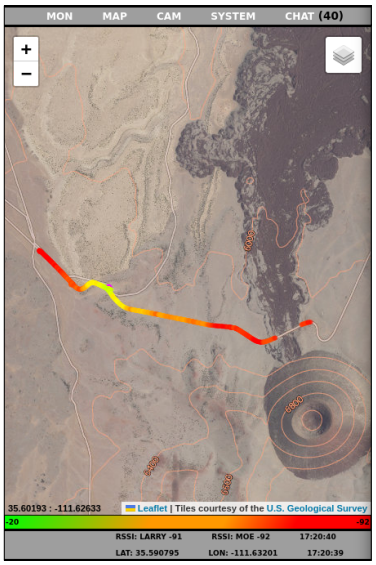


(d) System

Fig. 14: Software user interface web pages. Map source: [19].



(a) Monitor



(b) Map

Fig. 15: Example software pages during a field test depicting a loss of communications event. The monitor page indicates a red failure for network connectivity and a yellow warning indicator for the minimum allowable signal strength. The communications link was dropped during the traverse of the lava flow, shown by the track discontinuity along the road on the right side of the map page. Map source: [19].

B. Test Summary

Site	Date [Y-M-D]	Time [UTC]	Duration [min]	Mobile Node	Distance [km]	Avg Speed [m/s]	Max Speed [m/s]	Avg RSSI [dBm]	Max RSSI [dBm]
Site F: West of Lava Flow	2022-10-14	20:23:50	37	Vehicle	5.61	4.9	15.9	-44	-42
	2022-10-14	21:13:03	35	Vehicle	8.71	8.1	18.8	-48	-45
	2022-10-14	22:09:19	27	Vehicle	7.14	8.4	18.7	-47	-45
	2022-10-15	16:45:35	23	Vehicle	2.05	2.9	14.2	-46	-44
	2022-10-15	17:12:45	27	Vehicle	7.98	9.7	16.3	-48	-45
	2022-10-15	17:39:49	25	Vehicle	7.99	10.5	17.2	-49	-46
	2022-10-15	18:39:09	81	Person	3.36	1.4	3.4	-41	-38
	2022-10-15	20:00:21	57	Person	1.09	0.7	3.0	-44	-41
	2022-10-15	20:57:41	52	Person	2.0	1.4	3.2	-44	-42
Site K: East of Lava Flow	2022-10-17	17:37:58	45	Vehicle	15.65	11.4	19.3	-45	-42
	2022-10-17	18:22:36	21	Vehicle	4.44	6.7	19.3	-47	-45
	2022-10-17	19:36:22	53	Person	2.26	1.5	3.2	-40	-37
	2022-10-17	20:43:22	112	Person	4.17	1.3	3.2	-40	-37
	2022-10-18	17:15:11	46	Person	1.84	1.4	3.2	-43	-40
	2022-10-18	18:10:51	110	Person	4.16	1.3	3.2	-41	-38
Site L: Canyon	2022-10-18	22:20:20	74	Person	1.71	0.9	4.7	-40	-37
	2022-10-19	16:02:51	95	Person	2.75	1.1	3.6	-41	-38
	2022-10-19	17:41:27	28	Person	1.2	1.5	2.9	-40	-38
	2022-10-19	20:14:37	98	Vehicle	4.33	1.5	3.5	-42	-39
	2022-10-19	22:45:43	38	Vehicle	11.67	10.0	23.7	-44	-41
Site A: Open Plains	2022-10-20	16:35:10	80	Vehicle	20.64	8.4	22.8	-44	-41
	2022-10-20	18:25:10	83	Person	2.77	1.2	4.2	-41	-38
Totals			21.3 hr		130.6 km				

TABLE III: Summary of conducted field tests